Dynamic mapping of human cortical development during childhood through early adulthood

Nitin Gogtay*†, Jay N. Giedd*, Leslie Lusk*, Kiralee M. Hayashi‡, Deanna Greenstein*, A. Catherine Vaituzis*, Tom F. Nugent III*, David H. Herman*, Liv S. Clasen*, Arthur W. Toga‡, Judith L. Rapoport*, and Paul M. Thompson‡

*Child Psychiatry Branch, National Institutes of Mental Health, National Institutes of Health, Bethesda, MD 20892; and ‡Laboratory of Neuro Imaging, Department of Neurology, University of California School of Medicine, Los Angeles, CA 90095-1769

Communicated by Leslie G. Ungerleider, National Institutes of Health, Bethesda, MD, April 15, 2004 (received for review January 7, 2004)

We report the dynamic anatomical sequence of human cortical gray matter development between the age of 4–21 years using quantitative four-dimensional maps and time-lapse sequences. Thirteen healthy children for whom anatomic brain MRI scans were obtained every 2 years, for 8–10 years, were studied. By using models of the cortical surface and sulcal landmarks and a statistical model for gray matter density, human cortical development could be visualized across the age range in a spatiotemporally detailed time-lapse sequence. The resulting time-lapse ''movies'' reveal that (*i*) higher-order association cortices mature only after lower-order somatosensory and visual cortices, the functions of which they integrate, are developed, and (*ii*) phylogenetically older brain areas mature earlier than newer ones. Direct comparison with normal cortical development may help understanding of some neurodevelopmental disorders such as childhood-onset schizophrenia or autism.

Human brain development is structurally and functionally a nonlinear process (1–3), and understanding normal brain maturation is essential for understanding neurodevelopmental disorders (4, 5). The heteromodal nature of cognitive brain development is evident from studies of neurocognitive performance (6, 7), functional imaging (functional MRI or positron-emission tomography) (8–10), and electroencephalogram coherence studies (1, 2, 10). Prior imaging studies show regional nonlinear changes in gray matter (GM) density during childhood and adolescence with prepubertal increase followed by postpubertal loss (11–14). The GM density on MRI is an indirect measure of a complex architecture of glia, vasculature, and neurons with dendritic and synaptic processes. Studies of GM maturation show a loss in cortical GM density over time (15, 16), which temporally correlates with postmortem findings of increased synaptic pruning during adolescence and early adulthood (17–19). Here we present a study of cortical GM development in children and adolescents by using a brain-mapping technique and a prospectively studied sample of 13 healthy children (4–21 years old), who were scanned with MRI every 2 years for 8–10 years. Because the scans were obtained repeatedly on the same subjects over time, statistical extrapolation of points in between scans enabled construction of an animated time-lapse sequence (''movie'') of pediatric brain development. We hypothesized that GM development in childhood through early adulthood would be nonlinear as described before and would progress in a localized, region-specific manner coinciding with the functional maturation. We also predicted that the regions associated with more primary functions (e.g., primary motor cortex) would develop earlier compared with the regions that are involved with more complex and integrative tasks (e.g., temporal lobe).

The result is a dynamic map of GM maturation in the pre- and postpubertal period. Our results, while highlighting the remarkable heterogeneity, show that the cortical GM development appears to follow the functional maturation sequence, with the primary sensorimotor cortices along with frontal and occipital poles maturing first, and the remainder of the cortex developing in a parietal-to-frontal (back-to-front) direction. The superior temporal cortex, which contains association areas that integrate information from several sensory modalities, matured last. Furthermore, the maturation of the cortex also appeared to follow the evolutionary sequence in which these regions were created.

Methods

Subjects. Sample demographics are shown in Table 1. All subjects were recruited from the community for an ongoing National Institute of Mental Health study of human brain development (20). Briefly, each subject was given a structured diagnostic interview to rule out any psychiatric diagnoses at each visit. Subjects returned every 2 years for a follow-up MRI together with psychiatric and neurocognitive reassessment. A subset of all children who had three or more usable MRI scans and were between the ages of 4 and 21 years was chosen to be included in this study. The study was approved by the National Institute of Mental Health institutional review board, and an informed consent was obtained from subjects >18 years old or from parents of minor subjects, and an additional written assent was obtained from each minor subject.

Image Processing and Analysis. MRI images were acquired at the National Institute of Mental Health on the same 1.5-T General Electric scanner. The MRI sequence was consistent throughout the study. T1-weighted images with contiguous 1.5-mm slices in the axial plane and 2.0-mm slices in the coronal plane were obtained by using 3D spoiled-gradient recalled echo in the steady state. Imaging parameters were: echo time, 5 ms; repetition time, 24 ms; flip angle, 45°; acquisition matrix, 256 × 192; number of excitations, 1; and field of view, 24 cm. With each major software/hardware upgrade, the reliability of the data before and after the upgrade was tested by scanning a set of subjects before and after the upgrade (20). Briefly, for each scan, a radio-frequency bias field-correction algorithm was applied. Baseline images were normalized, transforming them to a standard 3D stereotaxic space (21). Follow-up scans were then aligned to the baseline scan from the same subject, and mutually registered scans for each subject were linearly mapped into the International Consortium for Brain Mapping (ICBM) space (22). An extensively validated tissue classifier generated detailed maps of GM, white matter, and cerebrospinal fluid by using a Gaussian mixture distribution to generate a maximum *a posteriori* segmentation of the data (23, 24), and a surface model of the cortex was then automatically extracted for each subject and time point as described (25).

An image-analysis technique known as cortical pattern matching (25–27) was used to better localize cortical differences over time and increase the power to detect systematic changes (25). This approach matches gyral features of cortical

Abbreviations: GM, gray matter; STG, superior temporal gyrus.

†To whom correspondence should be addressed at: Child Psychiatry Branch, National Institute of Mental Health, Building 10, Room 3N 202, Bethesda, MD 20892. E-mail: nitin@codon.nih.gov.

Table 1. Demographics of the study sample

No. of subjects	13
Gender (no. of male:female)	6:7
Total no. of scans	52
Average age (±SD) at	
Scan 1	9.8 ± 3.8 years
Scan 2	11.7 ± 4.1 years
Scan 3	13.8 ± 4.4 years
Scan 4	16.7 ± 4.3 years
Average age for all scans	13.0 ± 4.8 years
Average IQ (±SD)	125.8 ± 12.7
Handedness (no. of right:left)	12:1

surface anatomy as far as possible across subjects before making cross-subject comparisons, group averages, and statistical maps. Because this technique eliminates some confounding anatomical variance, there is increased statistical power for detecting statistical effects on cortical measures as well as increased ability to localize these effects relative to major sulcal and gyral landmarks. In the cortical matching step, secondary deformations are computed that match gyral patterns across all the time points and all subjects, which allows data to be averaged and compared across corresponding cortical regions. A set of 34 sulcal landmarks per brain constrains the mapping of one cortex onto the other by using corresponding cortical regions across subjects. An image analyst blind to subject identity, gender, and age traced each of 17 sulci in each lateral hemisphere on the surface rendering of each brain. These sulci included the Sylvian fissure, central, precentral, and postcentral sulci, superior temporal sulcus (STS) main body, STS ascending branch, STS posterior branch, primary and secondary intermediate sulci, and inferior temporal, superior, and inferior frontal, intraparietal, transverse occipital, olfactory, occipitotemporal, and collateral sulci. In addition to contouring the major sulci, a set of six midline landmark curves bordering the longitudinal fissure was outlined in each hemisphere to establish hemispheric gyral limits. Landmarks were defined according to a detailed anatomical protocol. This protocol is available on the Internet (www.loni.ucla.edu/~khayashi/Public/medial_surface) and has known inter- and intrarater reliability as reported (25).

A time-dependent average 3D cortical model for the group was created by flattening all sulcal/gyral landmarks into a 2D plane along with the cortical model assigning a color code to retain 3D shape information. Once data were in this flat space, sulcal features were aligned across subjects to an average set of sulcal curves. The warped cortical maps were mathematically reinflated to 3D, producing a crisp average cortical model with gyral features in their mean anatomic locations (28).

To quantify local GM, we used a measure termed "GM density," used in many prior studies, which measures the proportion of GM in a small region of fixed radius (15 mm) around each cortical point (15, 25, 26, 28). The GM-density measure averages information on GM volumes over a small neighborhood (the 15-mm kernel used in this report), providing an increased signal-to-noise ratio, and it averages away some of the noise inherent in resolving the cortical GM boundaries in MRI. However, if GM density is used, some localization power is lost, and the approach can average data from opposing sulcal banks. The measure also can index GM changes stemming from differences in cortical surface curvature, in which increased curvature may cause less GM to be sampled within the kernel of a fixed radius. Our work, however, shows that GM density and thickness are very highly correlated (K. Narr, R. M. Bilder, A. W. Toga, R. P. Woods, D. E. Rex, P. Szeszko, D. Robinson, Y. Wang, H. DeLuca, D. Asuncion, and P. M. Thompson, unpublished data) and therefore likely index similar maturational processes.

To determine whether there was enough power to achieve statistical significance at each surface point on the cortex, we fitted the model of GM change and estimated the multiple regression coefficient (R^2) at each point, which varies in the range of 0 to 1. From the null distribution of R^2, adjusted for the number of degrees of freedom in the statistical model, it is possible to determine whether there is sufficient power to reject the null hypothesis ($R^2 = 0$) at each cortical point. The significance of the model fit, $p(R^2)$, then was plotted at each cortical point (data not shown). The resulting map indicated that R^2 is not zero at almost every cortical point, suggesting that the changes seen were very highly significant.

Statistical plots were generated by using a mixed-model regression analysis (11, 30) for the GM volumes at each of 65,536 points on the entire cortical surface as well as individual lobar volumes and also at several specific points of interest over the surface. Because a nonlinear mixed model was used, intersubject differences in GM density were modeled separately from the intraindividual rates of cortical change, giving additional power to resolve longitudinal changes at each cortical point. Hypothesis tests for model building were based on F statistics with $\alpha = 0.05$. Specifically, F tests were used to determine whether the order of a developmental growth model was cubic, quadratic, or linear. If a cubic model was not significant, a quadratic model was tested; if a quadratic model was not significant, a linear model was tested. Thus a growth model was polynomial/nonlinear if either the cubic or quadratic term significantly contributed to the regression equation. Given that each hypothesis was tested only once, correction of the statistics for multiple comparisons was not necessary.

The following regions were selected for analyses in each hemisphere: precentral gyrus, primary motor cortex (Fig. 1A), superior frontal gyrus, posterior limit near the central sulcus (Fig. 1B), inferior frontal gyrus, posterior limit (Fig. 1C), inferior frontal sulcus, anterior limit (Fig. 1D), inferior frontal sulcus in the dorsolateral prefrontal cortex (Fig. 1E), anterior end of superior frontal sulcus (Fig. 1F), frontal pole (Fig. 1G), primary sensory cortex in postcentral gyrus (Fig. 1H), supramarginal gyrus (area 40) (Fig. 1I), angular gyrus (area 39) (Fig. 1J), occipital pole (Fig. 1K), anterior, middle, and posterior portions of superior temporal gyrus (STG) (Fig. 1 L–N), inferior temporal gyrus midpoint, as well the anterior and posterior limits (Fig. 1 O–Q), and on the inferior surface, anterior and posterior ends of olfactory sulcus (Fig. 2 R and S) and the anterior and posterior ends of collateral sulcus (Fig. 2 T and U). Corresponding points were chosen on both hemispheres by using the same sulcal landmarks.

Results

Overall, the total GM volume was found to increase at earlier ages, followed by sustained loss starting around puberty. However, as seen in the time-lapse sequence (Figs. 2 and 3), the process of GM loss (maturation) begins first in dorsal parietal cortices, particularly the primary sensorimotor areas near the interhemispheric margin, and then spreads rostrally over the frontal cortex and caudally and laterally over the parietal, occipital, and finally the temporal cortex. (This sequence is available in Movies 1–4, which are published as supporting information on the PNAS web site.) Frontal and occipital poles lose GM early, and in the frontal lobe, the GM maturation ultimately involves the dorsolateral prefrontal cortex, which loses GM only at the end of adolescence.

To examine further the maturation patterns within individual cortical subregions, we used mixed-model regression analyses to construct plots of linear as well as nonlinear (quadratic or cubic) age effects on GM volumes at points of interest along the cortical

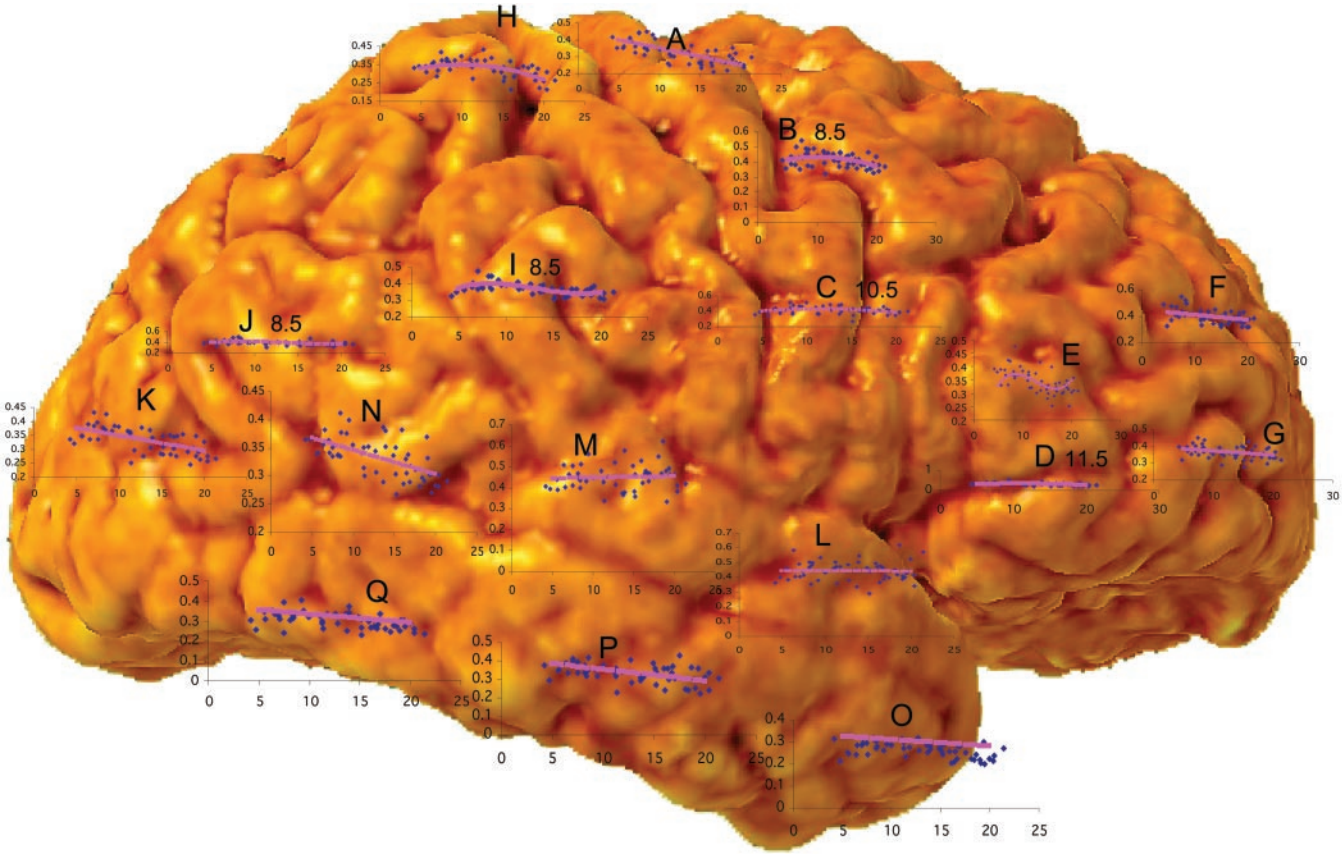

Fig. 1. Mixed-model regression plots at regions of interest over the cortical surface. The following regions were selected for analyses in each hemisphere: A, precentral gyrus and primary motor cortex; B, superior frontal gyrus, posterior end near central sulcus; C, inferior frontal gyrus, posterior end; D, inferior frontal sulcus, anterior end in the ventrolateral prefrontal cortex; E, inferior frontal sulcus in the dorsolateral prefrontal cortex; F, anterior limit of superior frontal sulcus; G, frontal pole; H, primary sensory cortex in postcentral gyrus; I, supramarginal gyrus (area 40); J, angular gyrus (area 39); K, occipital pole; L–N, anterior, middle, and posterior portions of STG; O–Q, anterior, middle, and posterior points along the inferior temporal gyrus anterior end. All quadratic, cubic, or linear terms were significant with $P < 0.05$. Age of peak GM is shown for B–D, I, and J. *x*-axis values are ages in years, and *y*-axis values show GM volumes.

surface by using major sulcal landmarks to ensure that corresponding anatomy was correlated correctly across time and subjects. When we compared the mean lobar volumes in this sample with our larger cross-sectional sample ($n = 149$), the trends for total and lobar GM volumes were in agreement in both groups (data not shown) (11). However, at individual subregions across the cortex, GM maturation shows a variable maturation pattern.

Within the frontal cortex, the precentral gyrus (Figs. 1A and 3) matures early. GM loss progresses linearly at an early age, whereas more rostral regions of the frontal lobe (along the superior and inferior frontal gyri; Figs. 1 and 3, B–G) mature successively in an anterior progression, as also indicated by the progressively later peaks of nonlinear GM loss (Fig. 1 B–D), with the prefrontal cortex maturing last (Figs. 1, D and E, and 3). In the parietal lobe, the GM loss begins in the postcentral gyrus (Figs. 1H and 3; with a nonlinear early peak), progressing laterally into the angular gyrus (area 40; Figs. 1I and 3), and supramarginal gyrus (area 39; Figs. 1J and 3). The frontal and occipital poles, similar to the pre- and postcentral gyri, mature early (Figs. 1 G and K and 3).

Later Maturation. Parts of the temporal lobe, on the other hand, show a characteristic late maturation pattern. The temporal lobe matures last except for the temporal pole, which shows GM loss around the same time as the frontal and occipital poles (Figs. 1O and 3). By contrast, the superior and inferior temporal gyri (STG and inferior temporal gyrus) do not show the same degree of GM loss throughout this age range. This is also shown by the flat graphs for age effects (Figs. 1 L and M and 3). Within the STG, the posterior part shows a distinct linear trajectory (Fig. 1N).

On the inferior brain surface, the medial aspects of the inferior temporal lobe (presumptive entorhinal cortex, medial to the rhinal sulcus, between the anterior end of the collateral sulcus and the posterior end of the olfactory sulcus) mature early and do not change much thereafter, as seen by the flat graphs for the age effects (Fig. 2T). A similar maturational pattern occurs in the caudal and medial parts of the inferior frontal lobe (Fig. 2S, presumptive piriform cortex). Other parts of the ventral temporal lobe show a lateral-to-medial pattern of maturation, whereas the orbitofrontal regions continued to mature until the oldest age that we studied (Fig. 2).

Discussion

Here we show a visualization of dynamic progression of human cortical brain development in a prospective, longitudinal study of healthy children and adolescents. Earlier reports have either been cross-sectional (i.e., an MRI scan is acquired only once per subject) or used methods that provide mean global volumes instead of point-by-point comparison that is possible with the mapping methods (11, 15). Cross-sectional designs are influenced by interindividual variance and cohort effects, whereas methods that provide mean global volumes provide no spatio-

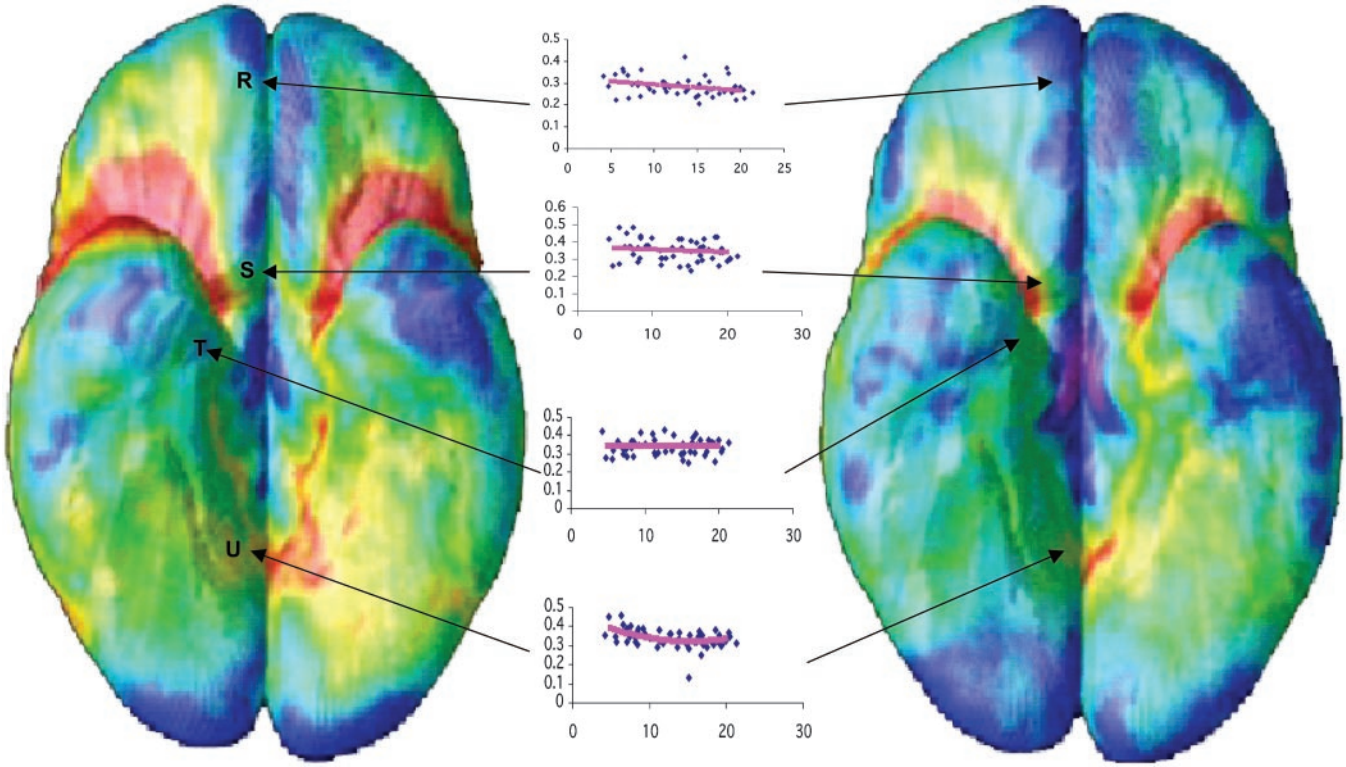

Fig. 2. Bottom view of the brain showing early and late time-lapse images. Points correspond to anterior and posterior ends of the olfactory sulcus (R and S) and collateral sulcus (T and U), and mixed-model graphs corresponding to the regions of interest on the right hemisphere are shown in the middle. *x*-axis values show ages in years, and *y*-axis values show GM volumes.

temporal detail. We have overcome these limitations by studying a longitudinally acquired pre- and postpubertal sample, in which the same children were rescanned prospectively over a 10-year period. Our results, while highlighting heterochronicity of human cortical development, suggest that individual subregions follow temporally distinct maturational trajectories in which higher-order association areas mature only after the lower-order sensorimotor regions, the functions of which they integrate, have matured. Additionally, it appears that phylogenetically older cortical areas mature earlier than the newer cortical regions.

Frontal-lobe maturation progressed in a back-to-front direction, beginning in the primary motor cortex (the precentral gyrus) and spreading anteriorly over the superior and inferior frontal gyri, with the prefrontal cortex developing last. Conversely, the frontal pole matured at approximately the same age as the primary motor cortex. In the posterior half of the brain, the maturation began in the primary sensory area, spreading laterally over the rest of the parietal lobe. Similar to the frontal pole, the occipital pole matured early. Lateral temporal lobes were the last to mature.

Thus, the sequence in which the cortex matured agrees with regionally relevant milestones in cognitive and functional development. Parts of the brain associated with more basic functions matured early: motor and sensory brain areas matured first, followed by areas involved in spatial orientation, speech and language development, and attention (upper and lower parietal lobes). Later to mature were areas involved in executive function, attention, and motor coordination (frontal lobes). The frontal pole, involved in taste and smell processing, and the occipital pole, containing the primary visual cortex, also matured early, as expected. This maturational sequence was also reflected in the peak ages for maximum GM values, which increase as development progresses anteriorly (Fig. 1 A–D and H–J). Visually, the prefrontal cortex and the inferior parietal cortex on the left side matured earlier than the corresponding regions on the right side, which may be because of the fact that the majority of children in this sample are right-handed, with a left-dominant hemisphere that matures early.

The temporal lobe followed a distinct maturation pattern. Temporal poles matured early. Most of the remaining temporal lobe matured during the age range of this sample except for a small area in the posterior part of the STG, which appeared to mature last. In humans, temporal cortex, in particular the posterior aspect of superior temporal sulcus, superior temporal gyrus, and middle temporal gyrus, is thought to be a heteromodal association site (along with prefrontal and inferior parietal cortices) and is involved with integration of memory, audiovisual association, and object-recognition functions (31–34). Thus, the temporal cortex continues to mature after other association areas, the functions of which it integrates, are relatively developed.

Phylogenetically, some of the oldest cortical regions lie on the inferior brain surface in the medial aspect of the temporal lobe (the posterior part of the piriform cortex and the entorhinal cortex, for example) or on the inferior and medial aspect of the frontal lobe near the caudal end of the olfactory sulcus (anterior piriform cortex and the orbital periallocortex) (35–37). The maturation process in the vicinity of these areas appeared to have started early (ontogenetically) already by the age of 4 years, as seen by the linear or flat plots (Fig. 2 S and T). From these areas, maturation slowly progresses laterally. In the inferior frontal cortex, the medial and posterior aspects of the olfactory cortices matured early, whereas orbitofrontal cortices matured later. In the remainder of the inferior temporal lobe, the maturation appeared later and in a somewhat lateral-to-medial direction. In mammals, the inferior temporal cortex, along with

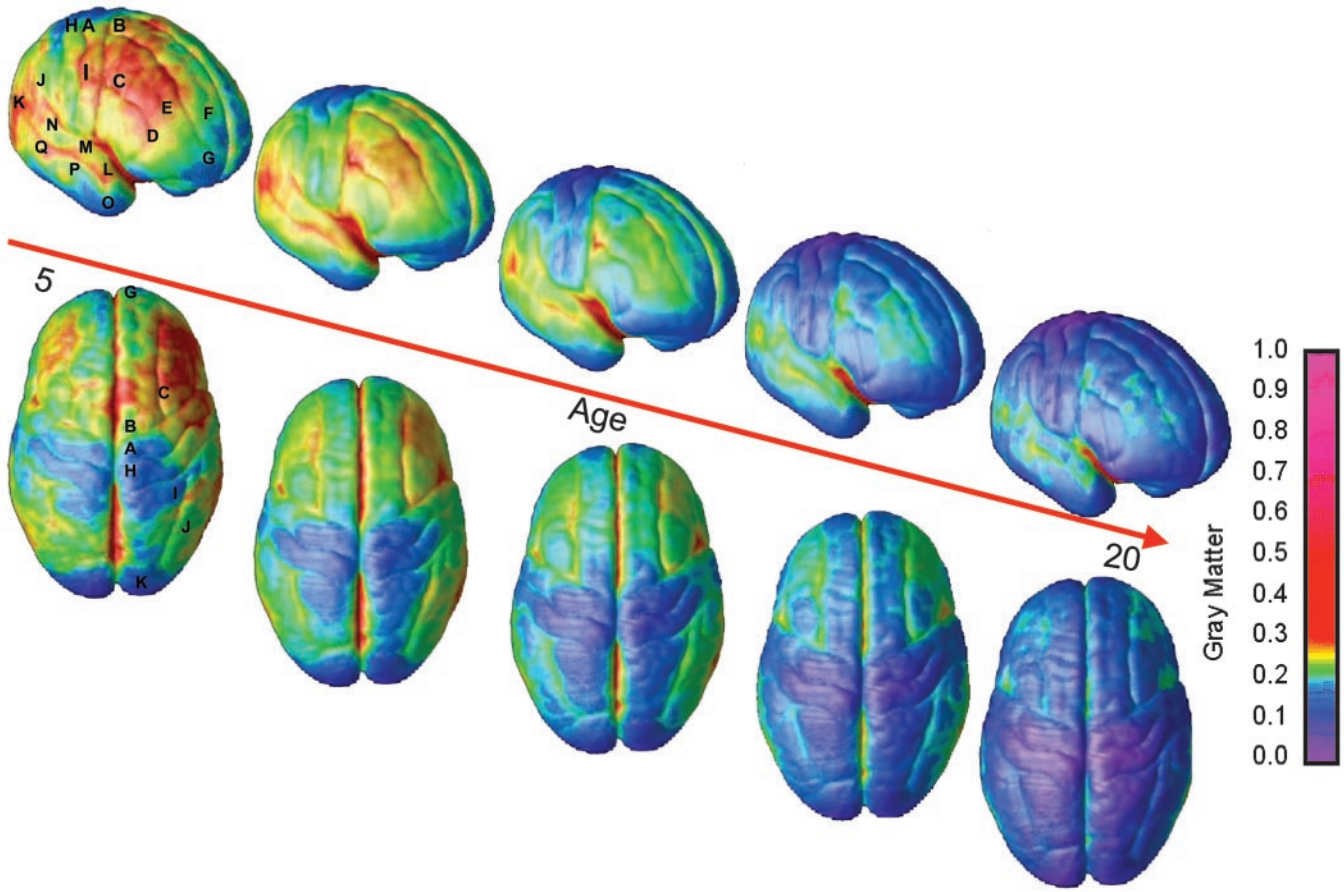

Fig. 3. Right lateral and top views of the dynamic sequence of GM maturation over the cortical surface. The side bar shows a color representation in units of GM volume. The initial frames depict regions of interest in the cortex as described for Fig. 1. This sequence is available in Movies 1–4 in the supporting information.

parts of the STG, posterior parietal cortex, and prefrontal cortex, are high-order association areas, which are also most recent evolutionarily (38, 39). Our observation of these areas appearing to mature later may suggest that the cortical development follows the evolutionary sequence to some degree.

The exact process underlying the GM loss is unknown. Cerebral white matter increases in the first four decades because of axonal myelination (40) and may partially explain the observed GM loss (41, 42). Although changes in sulcal and gyral folding patterns or other nonatrophic processes such as dehydration could influence the GM density, the primary cause for loss of GM density is unknown. We speculate that it may be driven at least partially by the process of synaptic pruning (43) together with trophic glial and vascular changes and/or cell shrinkage (44). Thus, region-specific differences in GM maturation may result from the underlying heterochronous synaptic pruning in the cortex, as has been shown in the primate and human cerebral cortical development (18, 45–48). Interestingly, in the frontal cortex, the dorsolateral prefrontal cortex matures last, coinciding with its later myelination, demonstrating that pruning myelination may often occur in parallel.

These findings may have clinical implications. For example, autism, with onset before the age of 3 years, shows global cerebral GM hyperplasia in the first 2 years of life (49) and larger frontal and temporal GM volumes by 4 years, followed by a slower rate of growth in these regions by 7 years (50, 51). Childhood-onset schizophrenia, with a mean age of onset around the age of 10 years, is associated with a striking parietal GM loss, which progresses anteriorly during adolescence in a back-to-front fashion (52), whereas adult-onset schizophrenia (the more typical form) is more strongly associated with deficits in later-maturing temporal and frontal regions (53–55) and is associated with selective abnormalities of the heteromodal regions (29). Thus, alterations either in degree or timing of basic maturational pattern may at least partially be underlying these neurodevelopmental disorders.

The magnitude of the changes in some cortical regions is highly significant and consistent with the growth and loss rates observed in our prior longitudinal studies. In an earlier report (28), we developed an approach using tensor mapping to measure the local growth rates and tissue-loss rates at a local level in the anatomy of the caudate and corpus callosum. In very small regions of these structures, local growth rates exceeded 40% per year, and local tissue-loss rates reached 40% per year in small regions of the basal ganglia. Because of the increased spatial resolution, peak local rates of change obtained from anatomical mapping approaches are often greater than those obtained in volumetric studies of anatomically parcellated brain structures. Assessment of lobar volumes, for example, can average growth or tissue-loss rates over a large structure, and the peak rates of volumetric change are reduced correspondingly. The cellular substrate for these cortical changes may be a combination of myelination, dendritic pruning, and changes in the neuronal, glial, vascular, and neurite packing density in different cortical laminae. There also may be changes in the relaxometric properties of the MRI signal, which is based on underlying water content. The myelination component can result in very large net percent changes in cortical volumes over periods of several years, especially when the volumes assessed are relatively small.

There are several limitations to this study. These analyses are based on 52 scans, in which 1,976 anatomical models were created, giving sufficient power to track change, but are from only13 children. In addition, this is a nonrepresentative population with an average IQ of 125, reflecting a referral bias of the National Institute of Mental Health study. We were not able to capture prepubertal gain in the time-lapse movie sequence, although it was readily visualized in the mixed-model graphs. Similarly, gender differences in brain maturation could not be explored, because there are only six males and seven females in the sample. However, our findings uncover key information on the maturational sequence of early brain development and its relation to functional and evolutionary milestones.

We thank Drs. Steven Wise (National Institutes of Health) and Alex Martin (National Institutes of Health) for valuable input and comments. This work was supported by National Institute of Mental Health Intramural funding; research grants from the National Institute for Biomedical Imaging and Bioengineering (EB 001561) and National Center for Research Resources (P41 RR13642 and R21 RR19771); and a Human Brain Project grant to the International Consortium for Brain Mapping, funded jointly by the National Institute of Mental Health and National Institute on Drug Abuse (P20 MH/DA52176).

1. Thatcher, R. W. (1992) *Brain Cognit*. **20,** 24–50.
2. Thatcher, R. W., Walker, R. A. & Giudice, S. (1987) *Science* **236,** 1110–1113.
3. Johnson, M. H. (2001) *Nat. Rev. Neurosci*. **2,** 475–483.
4. Stiles, J. (2000) *Dev. Neuropsychol*. **18,** 237–272.
5. Schlaggar, B. L., Brown, T. T., Lugar, H. M., Visscher, K. M., Miezin, F. M. & Petersen, S. E. (2002) *Science* **296,** 1476–1479.
6. Cepeda, N. J., Kramer, A. F. & Gonzalez de Sather, J. C. (2001) *Dev. Psychol*. **37,** 715–730.
7. Tamm, L., Menon, V. & Reiss, A. L. (2002) *J. Am. Acad. Child. Adolesc. Psychiatry* **41,** 1231–1238.
8. Luna, B., Thulborn, K. R., Munoz, D. P., Merriam, E. P., Garver, K. E., Minshew, N. J., Keshavan, M. S., Genovese, C. R., Eddy, W. F. & Sweeney, J. A. (2001) *Neuroimage* **13,** 786–793.
9. Chugani, H. T., Phelps, M. E. & Mazziotta, J. C. (1987) *Ann. Neurol*. **22,** 487–497.
10. Meyer-Lindenberg, A. (1996) *Electroencephalogr. Clin. Neurophysiol*. **99,** 405–411.
11. Giedd, J. N., Blumenthal, J., Jeffries, N. O., Castellanos, F. X., Liu, H., Zijdenbos, A., Paus, T., Evans, A. C. & Rapoport, J. L. (1999) *Nat. Neurosci*. **2,** 861–863.
12. Sowell, E. R., Thompson, P. M., Tessner, K. D. & Toga, A. W. (2001) *J. Neurosci*. **21,** 8819–8829.
13. Jernigan, T. L., Trauner, D. A., Hesselink, J. R. & Tallal, P. A. (1991) *Brain* **114,** 2037–2049.
14. Jernigan, T. L. & Tallal, P. (1990) *Dev. Med. Child Neurol*. **32,** 379–385.
15. Sowell, E. R., Peterson, B. S., Thompson, P. M., Welcome, S. E., Henkenius, A. L. & Toga, A. W. (2003) *Nat. Neurosci*. **6,** 309–315.
16. Sowell, E. R., Thompson, P. M., Holmes, C. J., Jernigan, T. L. & Toga, A. W. (1999) *Nat. Neurosci*. **2,** 859–861.
17. Huttenlocher, P. R. (1994) in *Human Behavior and the Developing Brain*, eds. Dawson, G. & Fischer, K. (Guilford, New York), pp. 137–152.
18. Bourgeois, J. P., Goldman-Rakic, P. S. & Rakic, P. (1994) *Cereb. Cortex* **4,** 78–96.
19. Rakic, P. (1996) in *Child and Adolescent Psychiatry*, ed. Lewis, M. (Williams and Wilkins, Baltimore), pp. 9–30.
20. Giedd, J. N., Snell, J. W., Lange, N., Rajapakse, J. C., Casey, B. J., Kozuch, P. L., Vaituzis, A. C., Vauss, Y. C., Hamburger, S. D., Kaysen, D., *et al*. (1996) *Cereb. Cortex* **6,** 551–560.
21. Sled, J. G., Zijdenbos, A. P. & Evans, A. C. (1998) *IEEE Trans. Med. Imaging* **17,** 87–97.
22. Collins, D. L., Neelin, P., Peters, T. M. & Evans, A. C. (1994) *J. Comput. Assist. Tomogr*. **18,** 192–205.
23. Shattuck, D. W. & Leahy, R. M. (2001) *IEEE Trans. Med. Imaging* **20,** 1167–1177.
24. Zijdenbos, A. P. & Dawant, B. M. (1994) *Crit. Rev. Biomed. Eng*. **22,** 401–465.
25. Thompson, P. M., Hayashi, K. M., de Zubicaray, G., Janke, A. L., Rose, S. E., Semple, J., Herman, D., Hong, M. S., Dittmer, S. S., Doddrell, D. M., *et al*. (2003) *J. Neurosci*. **23,** 994–1005.
26. Thompson, P. M., Mega, M. S., Vidal, C., Rapoport, J. L. & Toga, A. (2001) *Detecting Disease-Specific Patterns of Brain Structure Using Cortical Pattern Matching and a Population-Based Probabilistic Brain Atlas, IEEE Conference on Information Processing in Medical Imaging (IPMI), UC Davis 2001* (Springer, Berlin).
27. Ashburner, J., Csernansky, J. G., Davatzikos, C., Fox, N. C., Frisoni, G. B. & Thompson, P. M. (2003) *Lancet Neurol*. **2,** 79–88.
28. Thompson, P. M., Giedd, J. N., Woods, R. P., MacDonald, D., Evans, A. C. & Toga, A. W. (2000) *Nature* **404,** 190–193.
29. Buchanan, R. W., Francis, A., Arango, C., Miller, K., Lefkowitz, D. M., McMahon, R. P., Barta, P. E. & Pearlson, G. D. (2004) *Am. J. Psychiatry* **161,** 322–331.
30. Giedd, J. N., Jeffries, N. O., Blumenthal, J., Castellanos, F. X., Vaituzis, A. C., Fernandez, T., Hamburger, S. D., Liu, H., Nelson, J., Bedwell, J., *et al*. (1999) *Biol. Psychiatry* **46,** 892–898.
31. Mesulam, M. M. (1998) *Brain* **121,** 1013–1052.
32. Calvert, G. A. (2001) *Cereb. Cortex* **11,** 1110–1123.
33. Martin, A. & Chao, L. L. (2001) *Curr. Opin. Neurobiol*. **11,** 194–201.
34. Mesulam, M. (2000) *Principles of Behavioral and Cognitive Neurology* (Oxford Univ. Press, New York).
35. Puelles, L. (2001) *Philos. Trans. R. Soc. London B* **356,** 1583–1598.
36. Puelles, L. & Rubenstein, J. L. (2003) *Trends Neurosci*. **26,** 469–476.
37. Rubenstein, J. L., Martinez, S., Shimamura, K. & Puelles, L. (1994) *Science* **266,** 578–580.
38. Allman, J., Hakeem, A. & Watson, K. (2002) *Neuroscientist* **8,** 335–346.
39. Fuster, J. M. (2002) *J. Neurocytol*. **31,** 373–385.
40. Bartzokis, G., Beckson, M., Lu, P. H., Nuechterlein, K. H., Edwards, N. & Mintz, J. (2001) *Arch. Gen. Psychiatry* **58,** 461–465.
41. Benes, F. M. (1989) *Schizophr. Bull*. **15,** 585–593.
42. Benes, F. M., Turtle, M., Khan, Y. & Farol, P. (1994) *Arch. Gen. Psychiatry* **51,** 477–484.
43. Huttenlocher, P. R. (1979) *Brain Res*. **163,** 195–205.
44. Morrison, J. H. & Hof, P. R. (1997) *Science* **278,** 412–419.
45. Rakic, P., Bourgeois, J. P. & Goldman-Rakic, P. S. (1994) *Prog. Brain Res*. **102,** 227–243.
46. Bourgeois, J. P. (1997) *Acta. Paediatr. Suppl*. **422,** 27–33.
47. Zecevic, N., Bourgeois, J. P. & Rakic, P. (1989) *Brain Res. Dev. Brain Res*. **50,** 11–32.
48. Huttenlocher, P. R. & Dabholkar, A. S. (1997) *J. Comp. Neurol*. **387,** 167–178.
49. Courchesne, E., Carper, R. & Akshoomoff, N. (2003) *J. Am. Med. Assoc*. **290,** 337–344.
50. Saitoh, O. & Courchesne, E. (1998) *Psychiatry Clin. Neurosci*. **52** Suppl, S219–S222.
51. Carper, R. A., Moses, P., Tigue, Z. D. & Courchesne, E. (2002) *Neuroimage* **16,** 1038–1051.
52. Thompson, P. M., Vidal, C., Giedd, J. N., Gochman, P., Blumenthal, J., Nicolson, R., Toga, A. W. & Rapoport, J. L. (2001) *Proc. Natl. Acad. Sci. USA* **98,** 11650–11655.
53. Shenton, M. E., Dickey, C. C., Frumin, M. & McCarley, R. W. (2001) *Schizophr. Res*. **49,** 1–52.
54. Gur, R. E., Cowell, P., Turetsky, B. I., Gallacher, F., Cannon, T., Bilker, W. & Gur, R. C. (1998) *Arch. Gen. Psychiatry* **55,** 145–152.
55. DeLisi, L. E., Stritzke, P., Riordan, H., Holan, V., Boccio, A., Kushner, M., McClelland, J., Van Eyl, O. & Anand, A. (1992) *Biol. Psychiatry* **31,** 241–254.